Med Biol Eng Comput (2009) 47:677–684
DOI 10.1007/s11517-009-0462-z

TECHNICAL NOTE

Phantom haptic device upgrade for use in fMRI

Ales Hribar · Blaz Koritnik · Marko Munih

Received: 20 March 2008 / Accepted: 9 February 2009 / Published online: 5 March 2009

Abstract This paper presents an upgrade of a Phantom Premium 1.5 haptic device for use within a functional magnetic resonance imaging (fMRI) environment. A special mechanical extension that allows the haptic device to operate at a safe distance from the high-density magnetic field of an fMRI scanner has been developed. Extended haptic system was subjected to a series of tests to confirm electromagnetic compatibility with the fMRI scanner, for which key results are presented. With this fMRI compatible haptic platform a human brain activation during controlled upper limb movements can be studied. A simple virtual environment reaching task was programmed to study brain motor control functions. At the end preliminary results of an ongoing neurophysiological study are presented.

Keywords Phantom haptic device · fMRI · Mechanical extension · Electromagnetic compatibility · Brain imaging · Reaching · Human motor control

1 Introduction

Magnetic resonance imaging (MRI) is a standard non-invasive tool used in clinical diagnostics and research into the human body. Over the past few years, functional MRI (fMRI) has proved to be indispensable in human brain research. The fMRI technique is based on the measurement of blood oxygen level-dependent signals for estimation of neural activity in the human brain [19]. Clinical studies [14, 25] have investigated human brain activation during voluntary upper limb movements. However, a controlled movement task could provide new insights into human motor control. To asses and control isotonic, isometric or any other form of arm activity, a device capable of generating and measuring forces and trajectories is needed. A haptic device is suitable for these and a span of other combined activities that depend on position, velocity and acceleration. To perform such tasks inside an fMRI scanner, an fMRI compatible haptic interface is required.

A device used inside an fMRI environment requires a high level of safety and electromagnetic compatibility [22]. There are three major difficulties that impose limits on the use of electromechanical devices inside fMRI scanners. The high magnetic flux density, which exceeds 1 T in modern fMRI scanners, makes the use of ferromagnetic materials impossible (missile effect). The high level radio-frequency electromagnetic field and the sensitivity of the scanner receiver coils limit the use of electronic circuits. With a typical diameter of 60 cm, there is also limited space within the scanner bore. These limitations make the design of an fMRI compatible device a challenging task.

Nevertheless, several fMRI compatible devices have been developed in the last decade. Toma and Nakai [25] and Chapuis et al. [3] reported on fMRI compatible force sensors and actuators. An fMRI compatible surgical robot with five degrees-of-freedom (DOF) for use inside an intra-operative fMRI scanner was introduced by Chinzei and Miller [4]. The robot is powered by ultrasonic motors. A pneumatic 5-DOF fMRI compatible manipulator for automatic brachytherapy seed placement has been developed

A. Hribar (✉) · M. Munih
Faculty of Electrical Engineering, Trzaska 25,
Ljubljana, Slovenia
e-mail: alesh@robo.fe.uni-lj.si

B. Koritnik
Division of Neurology, Institute of Clinical Neurophysiology,
University Medical Centre Ljubljana, Zaloska 7,
Ljubljana, Slovenia

by Patriciu et al. [20]. There has also been an attempt to use a spherical ultrasonic motor to drive a 3-DOF fMRI compatible robot [15].

Research in the field of human motor control requires a tool capable of dynamically controlling arm and hand movements inside an fMRI scanner. Recently a few such devices have been developed. fMRI compatible hand rehabilitation devices were introduced by Khanicheh et al. [12, 13]. Simple 1-DOF haptic interfaces have also been reported [12, 13, 27, 9]. Different types of motors are used to drive these devices. More sophisticated haptic devices have been described [10, 11], one of which has 2-DOF and uses hydraulic actuators to generate force [10]. Another 2-DOF haptic device is powered by an ultrasonic motor [11]. In [16] authors discuss research directions for combined use of virtual reality and fMRI.

However, to the best to our knowledge, no 3-DOF haptic interface has been introduced to an fMRI environment to date. An important issue in fMRI experiments is the ability to imitate reality as closely as possible inside the scanner. A three-dimensional virtual environment represents a good approach. This motivated us to upgrade the Phantom Premium 1.5 haptic device to work inside an fMRI scanner room. Employing this widely accepted haptic device enabled us to use the existing software, thus accelerating design of the system. A mechanical carbon-fiber extension with a 3-DOF joint has been developed and coupled to the end-effector of the Phantom haptic device. This ensures that the Phantom can operate at a safe distance, well outside the high magnetic field of the main coil of the fMRI scanner.

A virtual environment that controls haptic and visual feedback has been programmed. This allows investigation of brain activation in human subjects during the execution of different virtual-environment tasks. The experiments presented in this paper were carried out on a Siemens Trio 3 T (Siemens Healthcare, Erlangen, Germany) fMRI scanner.

2 Methods and materials

2.1 Phantom premium 1.5

Phantom Premium 1.5 (SensAble Technologies, Inc., Woburn, MA) is a commercially available 3-DOF haptic device. It has already been used in our laboratory to study upper limb movements [1]. This was the main reason to use this, among research community, widely accepted haptic device. We were also trying to incorporate as much of the developed software as possible.

The Phantom has an adequate workspace of 381 mm × 267 mm × 191 mm and maximum exertable force of 8.5 N [24]. It's small size and light weight enabled us to quickly mount it on and off the support structure used in fMRI experiment.

2.2 Haptic system

The Phantom is driven by electric coreless motors. For a small electric motor operating inside the fMRI examination room, the maximum permitted magnetic flux density generated by the scanner is 3 mT [23]. Data supplied by Siemens suggested that the Phantom would have to be at a distance of 3 m away from the center of the magnet to meet this requirement. Additional measurements of the magnetic flux density were carried out to determine the exact position for the Phantom inside the scanner room. These measurements confirmed that the Phantom would need to be coupled using a 2 m long extension between the end-effector of the Phantom and the subject's hand to satisfy the maximum magnetic flux density.

The mechanical extension shown in Fig. 1 comprises two carbon fiber rods, a 2-DOF gimbal, and a linear rail with a carriage. A specially fabricated aluminum part with an $M22 \times 1.5$ thread is glued to the end of each carbon fiber rod. The rods are screwed into a gimbal cylinder, which is mounted on a main gimbal frame using a bronze

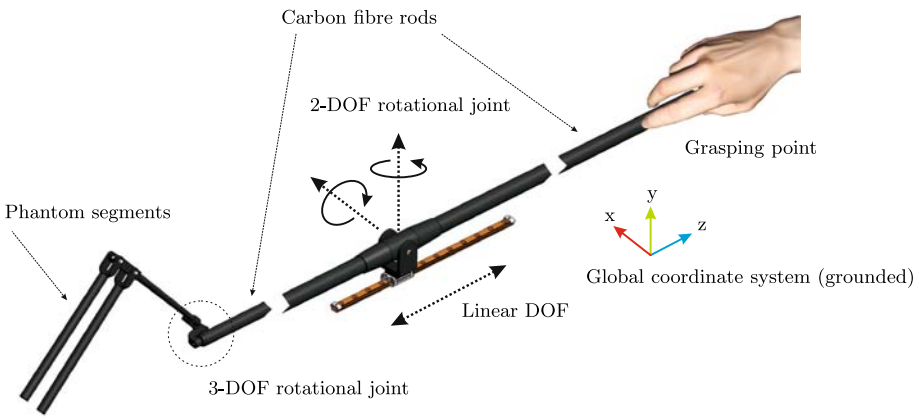

Fig. 1 Mechanical extension with a 3-DOF joint in the middle. Note that only parts of the carbon fiber rods are shown

axle and Teflon bearings. The main gimbal frame rotates on the bronze shaft mounted on the rail carriage. Non-ferromagnetic stainless steel hex screws are used to secure both axles. The final assembly gives the mechanical extension 3-DOF. The linear rail with the carriage provides a translational DOF and the gimbal adds two rotational DOF.

The stainless steel rail and RSR9ZM carriage were purchased from THK (THK Company Ltd., Tokyo, Japan). The 2-DOF aluminum gimbal was designed in Autodesk Inventor (Autodesk Inc., San Rafael, CA) and fabricated in a CNC machine shop.

One end of the mechanical extension is coupled to the Phantom haptic device. A 3-DOF rotational joint is used to connect Phantom and the extension, which are fixed on an aluminium frame that is assembled out of Bosch Rexroth (Bosch Rexroth AG, Lohr, Germany) aluminium strut profiles. The aluminum frame is bolted together with non-ferromagnetic stainless steel screws. A special plastic part was fabricated to connect the sliding examination table of the fMRI scanner and the aluminum frame. The assembly is shown in Fig. 2.

Phantom's electric motors and encoders are connected to a controller located outside examination room through two separate LIYCY shielded cables. No additional filtering is provided.

The virtual environment in which a human subject performs the desired arm movement task comprises haptic and visual parts. The Phantom device coupled to the mechanical extension enables the subject to execute the haptic part of the task. To ensure visual feedback, a projector and a projection screen were used. The beam of light coming from the projector enters the scanner room through a window. It is then reflected from the mirror and back-projected to the projection screen.

2.3 Physical properties of the extension

When the mechanical extension is used together with the Phantom haptic device a transformation between the Phantom base coordinate system and the extended haptic system coordinate system (marked in Fig. 1) occurs. X and y coordinate transforms to $-x$ and $-y$, respectively. For small displacements in x and y direction (with respect to

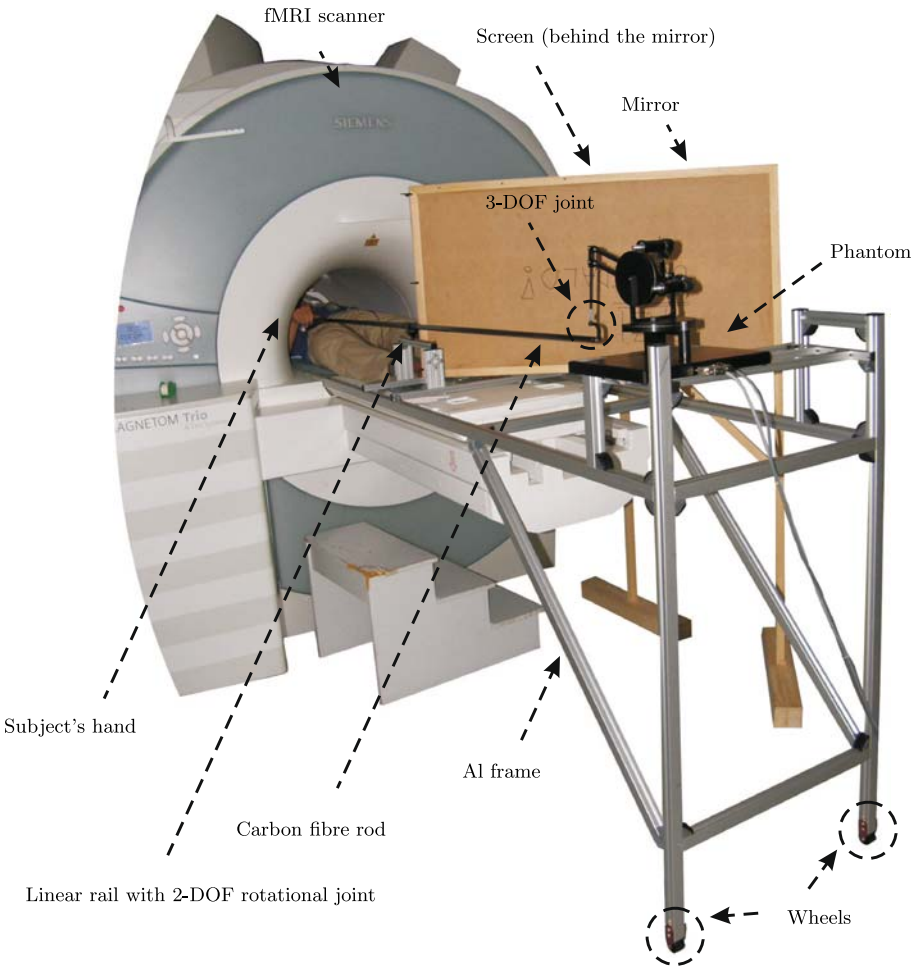

Fig. 2 Phantom haptic device coupled to the mechanical extension inside an fMRI scanner room. Haptic system is mounted on the aluminum construction

the length of the extension) z coordinate stays the same. The Phantom's original range of motion is not affected by the use of the extension. The 3-DOF joint comprises two carbon fibre rods of the same length which means that the magnitude of the maximal force produced by the Phantom does not change.

The mass (m_{ext}) and mass moments of inertia (I_{ext}) of the mechanical extension were estimated using the physical iProperties dialog box of Autodesk Inventor. The estimated mass value was compared with the mass measured using a precision weighing machine. The difference between these two mass values was less than 1%.

$$m_{\text{ext}} = 204 \times 10^{-3}\,\text{kg} \tag{1}$$

$$I_{\text{ext}} = \begin{bmatrix} 3.13 & 0 & 0 \\ 0 & 3.13 & 0 \\ 0 & 0 & 0 \end{bmatrix} \times 10^{-2}\,\text{kg}\,\text{m}^2 \tag{2}$$

2.4 Experimental software

Our goal was to develop haptic and visual virtual environment task whereby a human subject would perform reaching movements. In a simple virtual environment room shown in Fig. 3 all walls have haptic stiffness of $2,000\frac{N}{m}$ and damping of $200\frac{Ns}{m}$. Haptic dimensions of the room are 140 mm × 100 mm × 80 mm. Position of a white cursor ball in the virtual environment room reflects position of the end-effector point of the extended haptic system. The virtual environment session comprised four tasks: rest before reaching (RR), target reaching (R), rest before extension (RE) and non-targeting arm extension (E).

During RR and RE task edges of the room are colored red and denote rest of the subject. Subject is instructed to observe room and not to perform any movements. When edges of the room turn green subject performs reaching (R task) and arm extension (E task) movements. It is essential that the subject feels the impact with the target located on the back wall during R and E.

A complete virtual-environment session consists of eight blocks, each containing four of the above-mentioned tasks. The duration of each block is 2 min, with 30 s for each task in the block.

2.5 Extended haptic system evaluation

2.5.1 Testing outside fMRI scanner

Functionality of the extended haptic device was first tested in a laboratory. The aim of this testing was to assess the impact of the mechanical extension on subject performance during execution of a virtual environment task using the extended device. For this experiment, a slightly modified virtual-environment task was programmed. On the back wall of the virtual environment room, a white square target was shown at a fixed position at random time intervals between 4 and 6 s. The subject was instructed to hit the target with the ball cursor as soon as it was shown on the back wall. The starting position for the cursor was in the middle of the edge formed by the bottom and front walls. After it was hit, the target disappeared. Each subject was challenged with 20 trials.

The experimental procedure comprised two parts. Each of five male subjects (age range 26–29 years) first executed the virtual environment task using only the Phantom haptic device. In the second part of the experiment, the mechanical extension was added to the Phantom and the same task was repeated. A log file containing the trajectories, forces, start and hit times for each subject was generated for every run.

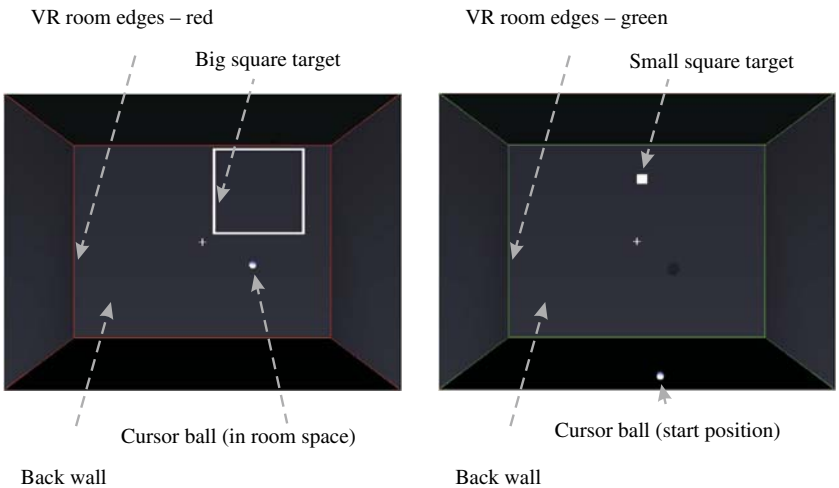

(a) Rest before extension **(b)** Reaching

Fig. 3 Virtual environment room during different trials

Comparison of average reaction and movement task execution times with and without the extension was made. A balanced one-way ANOVA (The ANalysis Of VAriance) test was applied to these two sets of data. Root square difference between average reaching trajectories with and without the extension was calculated. Mean and variance values of the root square difference vector were also computed.

Using the mass (Eq. 1) and the mass moment of inertia (Eq. 2) forces induced by the extension in the free space of virtual environment room were calculated for all three dimensions.

2.5.2 *Electromagnetic compatibility*

To investigate the electromagnetic compatibility of the extended haptic system, a series of tests were carried out. First, we observed the effect of the fMRI scanner on the extended haptic system. Extended haptic system was installed in the the fMRI examination room. The Phantom was connected to the controller and the virtual environment task was started. Meanwhile a echo planar (EPI) fMRI sequence with T_R = 3,000 ms, T_E = 30 ms, FOV = 192 mm, 36 slices, 6 mm slice thickness, 3 × 3 × 3 mm^3 voxel size was ran on the fMRI scanner. Any possible disturbance in the Phantom's operation has been observed.

Next step was to examine the influence of operation of the extended haptic system on the fMRI scanner. A cylindrical phantom object—not to be confused with the Phantom haptic device—(plastic bottle 1,900 ml, per 1,000 g H_2O dist.: 3.75 g $NiSO_4 \times 6H_2O$ + 5 g NaCl) was placed inside the fMRI scanner in the place where the subject's head usually lies. With no haptic device present inside the examination room a set of reference fMRI images was acquired. Then the extended haptic device was placed inside the examination room and two more sets were acquired. First set with the Phantom turned off and second set with the virtual environment task active. A volunteer inside the fMRI examination room, but outside the scanner was manipulating with the extended haptic device while acquiring second set of images. The fMRI sequence parameters were fixed throughout all three phases of the test and were the same as in the experiment described in the previous paragraph.

Signal-to-noise ratios (SNR) for two sets of acquired images were calculated according to [18].

2.5.3 *fMRI trial experiment*

A 15 min training session in which subject got used to the system was ran before the fMRI trial. The subject exercised with the same virtual environment task as later in the trial. During the fMRI experiment functional images were acquired using EPI fMRI sequence described earlier. The total scanning time was 6 min and 320 whole-brain functional images were acquired. All of the image analysis, including realignment, normalization, smoothing and statistical analysis based on a general linear model [8], was performed using Statistical Parametrical Mapping implemented in MATLAB (The MathWorks, Inc., Natick, MA). The four tasks (see above) were modeled as box car functions convolved with the hemodynamic response functions. After estimation of all model parameters, differences between the tasks were assessed by applying the following linear contrasts to the parameter estimates: R–RR, E–RE and R–E. A voxel threshold of $P < 0.05$ (corrected for multiple comparisons) was used for R–RR and E–RE, whereas an uncorrected threshold of $P < 0.001$ was used for the R–E comparison.

3 Results

3.1 Testing outside fMRI scanner

Comparison of the reaching trajectories, velocities and accelerations with and without the mechanical extension are presented in Fig. 4a–c, respectively. Each trace represents an average of 20 trajectories captured from one subject. For demonstration purposes and clarity, only one coordinate is presented in each plot: x for trajectories, y for velocities and z for accelerations. The coordinate system is marked in Fig. 1. Calculated mean and variance values of the root square difference between average reaching trajectories are 2.6 mm and 4.7 mm^2, respectively. Forces induced by the mechanical extension are presented in Fig. 4.

In Table 1 a comparison of reaching and movements times together with it's ANOVA test parameters is given.

3.2 Electromagnetic compatibility

No disturbances in the operation of the Phantom haptic device were detected in the first or in any of the following test experiments. Calculated SNR of fMRI images was higher than 170 for both studied cases. Acquired images did not reveal any abnormalities during visual inspection of trained personnel.

3.3 Functional trial

Comparison of reaching to the rest reaching task (R–RR) revealed activations in the left primary sensorimotor cortex (SM1), bilateral premotor cortex (PMC), inferior frontal gyrus (IFG), supplementary motor area (SMA), inferior and superior posterior parietal cortex (PPC), visual cortex,

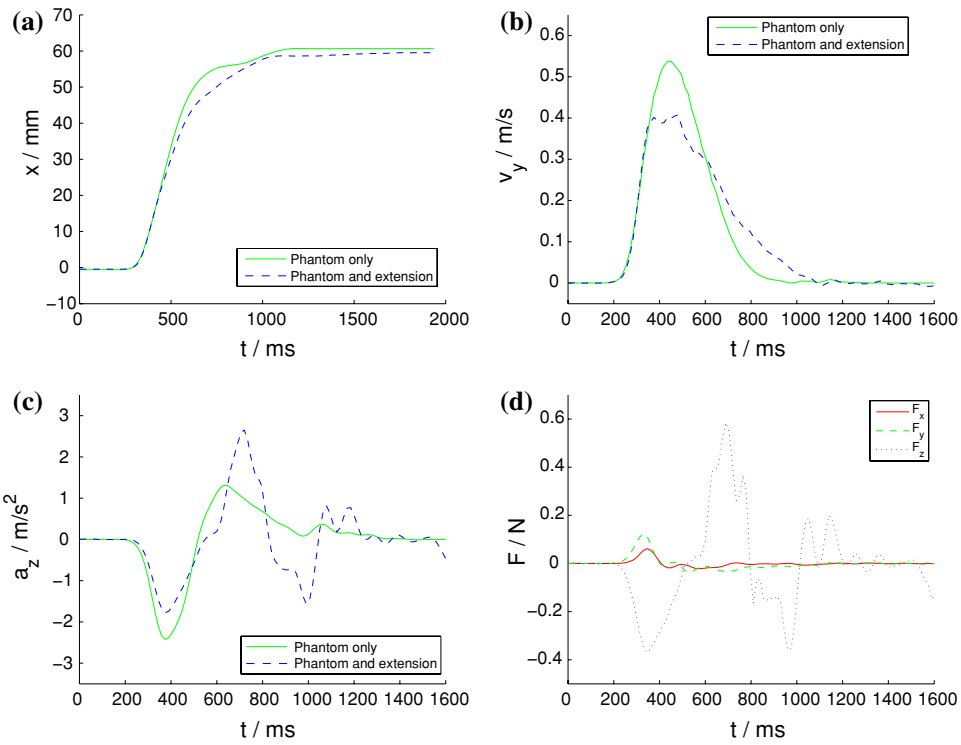

Fig. 4 Comparison of (**a**) trajectories, (**b**) velocities and (**c**) accelerations with (*dashed line*) and without (*full line*) the mechanical extension during evaluation of the reaching task outside the MRI scanner. **d** Forces induced by the mechanical extension. The coordinate system is marked in Fig. 1

Table 1 Average reaction and movement times (in ms)

Mode	$T_{Reaction}$	$T_{Movement}$	T_{Total}
Phantom only	310	770	1080
System	315	780	1095
F	0.04	0.84	0.57
p	0.85	0.39	0.47

left basal ganglia (BG) and predominantly the right cerebellar hemisphere (Fig. 5a). During non-targeted arm extension (E–RE), similar but less prominent brain activations were found, including right SM1, bilateral PMC, IFG, SMA, inferior PPC, visual cortex and right CRB. Direct comparison of reaching to arm extension (R–E) revealed that areas showing greater activation during R were the bilateral prefrontal cortex, SMA, right visual cortex and right CRB Fig. 5.

4 Discussion

Maximum force induced by the extension, which appears when moving extension in z direction, has insignificant effect on subject performance during the execution of the virtual environment task. This is also confirmed by the comparison of presented reaching trajectories and reaction times.

These results demonstrate that there is no notable difference in subject performance when the simple virtual environment task is executed using the Phantom device coupled to the mechanical extension, compared to execution without the extension. Results apply only to the presented virtual environment task and can not be directly generalized to other applications.

During the compatibility tests no disturbance in the operation of the Phantom haptic device or fMRI scanner were observed. Due to the fact that ferromagnetic electromechanical parts are present in the examination room, the extended haptic system can be, according to [21], labeled as “MR-conditional”.

5 Conclusions

This paper presents the upgrade and testing of a Phantom haptic device for use in fMRI environment. We were able to achieve electromagnetic compatibility of the extended haptic device without changing any of Phantom’s original mechanical or electrical components. The mechanical extension and the 3-DOF joint allows the Phantom device to work outside the 3 mT magnetic flux density line. The Phantom haptic device coupled to the mechanical extension was subjected to a series of tests that confirmed its electromagnetic and functional compatibility with the fMRI environment. A cylindrical phantom object was scanned and other measurements were utilized in fMRI compatibility tests. Tests outside the fMRI scanner also confirmed that the mechanical extension has a negligible

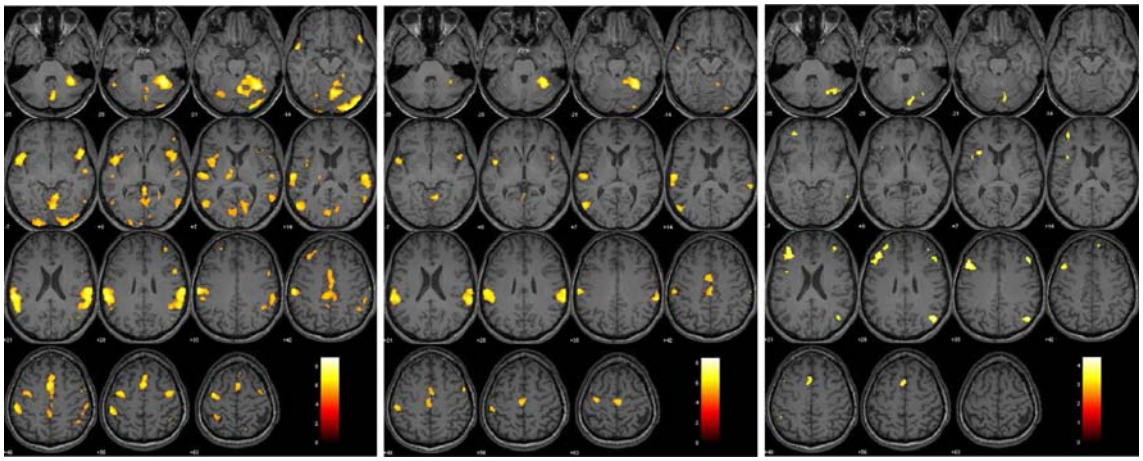

(a) Brain activation during reaching compared to rest

(b) Brain activation during non-targeting arm extension compared to rest

(c) Brain areas that showed greater activation during reaching compared to arm extension.

Fig. 5 fMRI maps showing brain areas activated during virtual environment tasks. Transverse slices with the right side of the brain on the right; *z* coordinates are shown below the slices and the *color bar* represents statistical *t* values

impact on the original Phantom dynamics. We have observed a bilateral sensorimotor brain network activation during the execution of the virtual environment task. The activations were greater during the reaching task compared to arm extension. A similar fronto-parietal network for reaching has been observed in other functional neuroimaging and electrophysiological studies [2, 5, 17].

References

1. Bardorfer A, Munih M, Zupan A, Primozic A (2001) Upper limb motion analysis using haptic interface. IEEE/ASME Trans Mechatron 6(3): 253–260
2. Chapman H, Gavrilescu M, Wang H, Kean M, Egan G, Castiello U (2002) Posterior parietal cortex control of reach-to-grasp movements in humans. Eur J Neurosci 15:2037–2042
3. Chapuis D, Gassert R, Sache L, Burdet E, Bleuler H (2004) Design of a simple MRI/fMRI compatible force/torque sensor. In: Proceedings of the 2004 IEEE/RSJ international conference on intelligent robots and systems
4. Chinzei K, Miller K (2001) MRI guided surgical robot. In: Proceedings of the 2001 Australian conference on robotics and automation
5. Desmurget M, Gréa H, Grethe JS, Prablanc C, Alexander GE, Grafton ST (2001) Functional anatomy of nonvisual feedback loops during reaching: a positron emission tomography study. J Neurosci 21:2919–2929
6. Di Diodato LM, Mraz R, Baker SN, Graham SJ (2007) A haptic force feedback device for virtual reality-fMRI experiments. IEEE Trans Neural Syst Rehabil Eng 15(4):570–576
7. Flueckiger M, Bullo M, Chapuis D, Gassert R, Perriard Y (2005) fMRI compatible haptic interface actuated with traveling wave ultrasonic motor. In: Proceedings of the 2005 industry applications conference, 40th IAS annual meeting, Vol. 3, pp 2075–2082
8. Friston KJ, Holmes AP, Worsley KJ, Poline JP, Frith CD, Frackowiak RSJ (1995) Statistical parametric maps in functional imaging: a general linear approach. Hum Brain Mapp 2:189–210
9. Gassert R, Moser R, Burdet E, Bleuler H (2006) MRI/fMRI-compatible robotic system with force feedback for interaction with human motion. IEEE/ASME Trans Mechatron 11:216–224
10. Gassert R, Dovat L, Lambercy O, Ruffieux Y, Chapuis D, Ganesh G, Burdet E, Bleuler H (2006) A 2-DOF fMRI compatible haptic interface to investigate the neural control of arm movements. In: Proceedings of the 2006 IEEE international conference on robotics and automation
11. Izawa J, Shimizu T, Aodai T, Kondo T, Gomi H, Toyama S, Ito K (2006). MR compatible manipulandum with ultrasonic motor for fMRI studies. In: Proceedings of the 2006 IEEE international conference on robotics and automation, Orlando
12. Khanicheh A, Muto A, Triantafyllou C, Weinberg B, Astrakas L, Tzika A, Mavroidis C (2006) fMRI-compatible rehabilitation hand device. J NeuroEng Rehab 3:24
13. Khanicheh A, Mintzopoulos D, Weinberg B, Tzika A, Mavroidis C (2007). MR_CHIROD v.2: a fMRI compatible mechatronic hand rehabilitation device. In: Proceedings of the 10th IEEE international conference on rehabilitation robotics
14. Lehericy S, Bardinet E, Tremblay L, Van de Moortele PF, Pochon JB, Dormont D, Kim DS, Yelnik J, Ugurbil K (2006) Motor control in basal ganglia circuits using fMRI and brain atlas approaches. Cereb Cortex 16:149–161
15. Mashimo T, Toyama S (2007) MRI compatibility of a manipulator using a spherical ultrasonic motor. In: Proceedings of the 12th IFToMM world congress
16. Mraz R, Hong J, Quintin G, Staines WR, McIlroy WE, Zakzanis KK, Graham SJ (2003) A platform for combining virtual reality experiments with functional magnetic resonance imaging. Cyberpsychol Behav 6(4):359–368
17. Naranjo JR, Brovelli A, Longo R, Budai R, Kristeva R, Battaglini PP (2007) EEG dynamics of the frontoparietal network during reaching preparation in humans. Neuroimage 34:1673–1682
18. NEMA Standards Publication MS 1-2001, Determination of Signal-to-Noise Ratio (SNR) in Diagnostic Magnetic Resonance Imaging.

19. Ogawa S, Menon RS, Kim SG, Ugurbil K (1998) On the characteristics of functional magnetic resonance imaging of the brain. Annu Rev Biophys Biomol Struct 27:447–474
20. Patriciu A, Petrisor D, Muntener M, Mazilu D, Schar M, Stoianovici D (2007) Automatic brachytherapy seed placement under MRI guidance. IEEE Trans Biomed Eng 54:1499–1506
21. Schaefers G (2008) Testing MR safety and compatibility. IEEE Eng Med Biol Mag 27(3):23–27
22. Schueler BA, Parrish TB, Lin JC, Hammer BE, Pangrle BJ, Ritenour ER, Kucharczyk J, Truwit CL (1999) MRI compatibility and visibility assessment of implantable medical devices. J Magn Reson Imaging 9:596–603
23. SIEMENS Medical Solutions (2006) MAGNETIC RESONANCE MAGNETOM Trio A Tim System, Technical Drawing
24. Specifications Comparison For The Phantom Premium 1.0, 1.5, 1.5 High Force, And 3.0 Haptic Devices. http://www.sensable.com/products-datasheets.htm
25. Toma K, Nakai T (2002) Functional MRI in human motor control studies and clinical applications. Magn Reson Med Sci 1:109–120
26. Vogan J, Wingert A, Plante JS, Dubowsky S, Hafez M, Kacher D, Jolesz F (2004) Manipulation in MRI devices using electrostrictive polymer actuators with an application to reconfigurable imaging coils. In: Proceedings of the 2004 IEEE international conference on robotics and automation, New Orleans
27. Yu N, Murr W, Blickenstorfer A, Kollias S, Riener R (2007) An fMRI compatible haptic interface with pneumatic actuation. In: Proceedings of the 10th IEEE international conference on rehabilitation robotics